RSC Advances

PAPER

View Article Online
View Journal | View Issue

Cite this: *RSC Adv.*, 2017, **7**, 21128

Cu@Ni core–shell nanoparticles/reduced graphene oxide nanocomposites for nonenzymatic glucose sensor†

Kong-Lin Wu,*[a] Ya-Miao Cai,[a] Bin-Bin Jiang,[b] Weng-Chon Cheong,[c] Xian-Wen Wei,*[a] Weizhi Wang[a] and Nan Yu[a]

Received 21st January 2017
Accepted 6th March 2017

DOI: 10.1039/c7ra00910k

rsc.li/rsc-advances

In this work, the $Cu_x@Ni_{100-x}$ core–shell nanoparticles (CSNPs) are deposited on reduced graphene oxide (rGO) sheets, and this nanocomposites (in a Nafion matrix) are shown to be a viable materials for nonenzymatic sensing of glucose. A novel nonenzymatic glucose sensor based on a glass carbon electrode modified with $Cu_{53}@Ni_{47}$ CSNPs/rGO (referred to as $Cu_{53}@Ni_{47}$ CSNPs/rGO/GCE) displays an enhanced electrocatalytic activity to glucose oxidation in 0.1 M NaOH solution than that of Cu/GCE, Ni/GCE, Cu/rGO/GCE, Ni/rGO/GCE, and $Cu_{52}@Ni_{48}$ CSNPs/GCE, respectively. This is attributed to the three-in-one synergetic effects from their bimetallic compositions, specific core–shell structures, and interactions from the bimetallic CSNPs and support materials of rGO sheets. At an applied potential of +0.575 V (*vs.* SCE), the electrode has a low detection limit (0.5 μM; S/N = 3), a very wide linear range (0.001 mM to 4.1 mM), high sensitivity (780 μA mM^{-1} cm^{-2}), and a fast response time (3 s). Thus, it has great potential for the development of nonenzymatic glucose sensors.

1 Introduction

The development of electrochemical glucose sensors has attracted considerable attention over the past few years because of the importance of fast and reliable glucose concentration determination in clinical diagnostics.[1] However, enzyme-modified electrodes have several disadvantages, namely, high enzyme costs, instability, complicated immobilization procedures, and critical operating conditions.[1] In order to resolve these problems, numerous efforts have focused on developing nonenzymatic electrodes. Various nanostructured metals, alloys, and metal oxides had been explored extensively because of their unique physical and chemical properties, such as increased surface area, fast mass transport, and notable catalytic activity.[2] Among these, non-noble metal Ni- or Cu-based nanomaterials exhibit remarkable electrocatalytic abilities for glucose.[3,4] However, pure metals, such as Ni and Cu, are difficult to prepare and have poor stability for electroanalysis because they readily oxidize in air and in solution.[5] Therefore, much more attention needs to be paid to develop Ni- or Cu-based nanostructures and their composites for improving the oxidation rate and stability of active materials.

On the one hand, the stability, chemical activity, and poisoning resistance of bimetallic or intermetallic compound electrode materials can be adjusted by controlling their morphologies, structures, compositions, or sizes. For instance, PdCu/GE,[6a] bilayer Ni/Cu porous nanostructured film,[6b] Ni–Cu/TiO_2 NTs,[6c] Ni/Cu/MWCNT,[6d] Cu–Co alloy dendrite,[6e] and Pt/Ni NWAs[6f] electrodes are prepared by different methods, and which all show a higher sensitivity for the quantitative determination of glucose than single-metal composite because of their large exposed area and excellent diffusion properties.[6] In recent years, nanoparticles (NPs) with core–shell (CS) structures are attracting attention because of their three major effects: ligand effect, ensemble effects, and geometric effects, which can be enhance the catalytic activities.[7]

On the other hand, carbon materials have been used as a matrix to enhance electron transfer rates and electrocatalytic activities.[8] As one important carbon material, graphene reveal a significant impact in fields of science and technology because of its remarkable physical and chemical properties.[9] The unique properties of graphene, such as remarkable surface area, excellent conductivity, and wide electrochemical range, make it an ideal material in electrochemical sensors.[10] For example, Ni–Co NSs/rGO[11a] and Cu–Co NSs/rGO–CHIT[11b] composites exhibit higher catalytic activities than their bimetallic nanostructures without graphene.

According to the previous reports, the catalytic performances of composites should be enhanced by alloy, bimetal, or

[a]*College of Chemistry and Materials Science, Key Laboratory of Functional Molecular Solids, The Ministry of Education, Anhui Laboratory of Molecule-based Materials (State Key Laboratory Cultivation Base), Anhui Key Laboratory of Functional Molecular Solids, Anhui Normal University, Wuhu 241000, China. E-mail: konglin@mail.ahnu.edu.cn; xwwei@mail.ahnu.edu.cn; Fax: +86-553-3869303; Tel: +86-553-3869303*

[b]*School of Chemical and Engineering, Anhui University of Technology, Maanshan 243002, China*

[c]*Department of Chemistry, Tsinghua University, Beijing 100084, China*

† Electronic supplementary information (ESI) available: Fig. S1–S5; Tables S1 and S2. See DOI: 10.1039/c7ra00910k

multimetallic, and suitable supports. These studies indicated that use of graphene-modified bimetallic electrodes resulted in well-performing glucose sensors. And yet for all that, the higher detection limit and narrower linear range of those sensors are observed.[6a,11a,b] Thereby, taking advantages of reduced graphene oxide sheets together with advanced features of the bimetallic Cu/Ni and its specific core–shell structure, which can enhance the electrocatalytic activity, biocompatibility, and sensitivity for biosensor applications.

Herein, we report a facile and one-pot solvothermal method to prepare of $Cu_x@Ni_{100-x}$ core–shell nanoparticles (CSNPs) decorated reduced graphene oxide (rGO) nanocomposites (NCs) (namely, $Cu_x@Ni_{100-x}$ CSNPs/rGO NCs). In this work, a series of enzymatic-free glucose sensors based on $Cu_x@Ni_{100-x}$ CSNPs/rGO NCs modified glassy carbon electrode (GCE), Cu/GCE, Ni/GCE, and $Cu_{52}@Ni_{48}$ CSNPs/GCE are constructed, and their electrochemical properties and electrocatalytic activities are investigated in details. What's exciting is that the $Cu_{53}@Ni_{47}$ CSNPs/rGO/GCE shows a good electrocatalytic performance for glucose oxidation, and which displays a lower detection limit (0.5 μM; S/N = 3), and a wider linear range (0.001 mM to 4.1 mM), high sensitivity (780 μA mM^{-1} cm^{-2}), and a fast response time (3 s), respectively.

2 Experimental

Chemicals and reagents

Glucose was purchased from Sinopharm Chemical Reagent Co. (China). Graphene oxide (GO) was purchased from Nanjing XFNANO Materials Tech Co. Ltd (China). Ultrapure water was used throughout the experiments. All reagents were of analytical grade and without further purifications.

Synthesis of $Cu_{53}@Ni_{47}$ CSNPs/rGO NCs

20 mg GO sheets was ultrasonically dispersed in 20 mL ethylene glycol (EG) for 5 h to form GO suspension. Then 20 mL EG solution including 0.5 mmol $CuCl_2 \cdot 2H_2O$ and 0.5 mmol $NiCl_2 \cdot 6H_2O$ was added drop wise the GO suspension under stirring to form a uniform dispersion. Subsequently, 5 mL EG solution with 0.01 mol NaOH was added dropwise into the above solution and being vigorously stirred for 1 h and then the mixture was transferred into a Teflon-lined stainless-steel autoclave with a capacity of 60 mL. The autoclave was sealed and put into a furnace, which was heated to and maintained at 200 °C for 5 h, and taken out and allowed to cool naturally to room temperature. Finally, the precipitates was collected by centrifugation and washed repeatedly with water and ethanol, and then vacuum dried for overnight and the $Cu_{53}@Ni_{47}$ CSNPs/rGO NCs were obtained. By the same conditions, the $Cu_x@Ni_{100-x}$ CSNPs/rGO NCs with different initial Cu/Ni molar ratios, Cu NPs, Ni NPs, and $Cu_{52}@Ni_{48}$ CSNPs were also prepared.

Characterization

The obtained samples were characterized by X-ray diffraction measurement (XRD, Shimadzu XRD-6000, Cu-Kα radiation, λ = 1.5406 Å), field emission scanning electron microscope (SEM, Hitachi S-4800) and transmission electron microscopy (TEM, FEI Tecnai G^2 20). The chemical compositions of final products were determined by inductively coupled plasma-atomic emission spectrometer (ICP-AES, Varian 710-ES) and X-ray photoelectron spectra (XPS, Thermo ESCALAB 250XI). Elemental mapping and high-angle annular dark field-scanning transmission electron microscope (HAADF-STEM) were carried out on a JEM-2100F microscope equipped with an energy-dispersive X-ray analysis system. All electrochemical experiments were performed with the CHI 660C (Chenhua, Shanghai) electrochemical workstation. A three electrode cell was used for the electrochemical experiments. The working electrodes were as-prepared $Cu_x@Ni_{100-x}$ CSNPs/rGO, Cu NPs, Ni NPs, and $Cu_{52}@Ni_{48}$ CSNPs/Nafion modified glassy carbon electrode (GCE, 3 mm in diameter) with a saturated calomel electrode (SCE) and a platinum wire as the reference auxiliary and the auxiliary electrode.

Preparation of modified electrode

A GCE was used as the conducting substrate for the development of the sensor platform. The GCE was carefully polished in 0.3 and 0.05 μm alumina slurry, respectively, and washed with ultrapure water followed by sonication in water. The catalyst suspension was prepared by dispersed 4 mg $Cu_x@Ni_{100-x}$ CSNPs/rGO NCs into 4 mL DMF containing 0.05% Nafion through ultrasonic treatment for 60 min. Then 6 μL of the corresponding suspension was coated on the GCE and dried in air to obtain sensors. For comparison, Cu NPs, Ni NPs, and $Cu_{52}@Ni_{48}$ CSNPs modified GCEs were also prepared by the same method.

3 Results and discussion

Material characterization

A facile and one-pot solvothermal method synthesis of $Cu_x@Ni_{100-x}$ CSNPs/rGO NCs is presented in this study. The hybrid NCs are prepared through the chemical reduction of Ni^{2+} and Cu^{2+} by using EG as a reducing agent at alkaline condition. Moreover, Cu NPs, Ni NPs, and $Cu_{52}@Ni_{48}$ CSNPs are also fabricated *via* the same procedures without GO sheets. Phase structure and purity of as-synthesized samples were examined *via* X-ray powder diffraction (XRD). Fig. 1 shows the typical XRD patterns of GO (Fig. 1A), Cu NPs (Fig. 1B), Cu/rGO (Fig. 1C), Ni NPs (Fig. 1D), and Ni/rGO (Fig. 1E), $Cu_{52}@Ni_{48}$ CSNPs (Fig. 1F), and $Cu_{53}@Ni_{47}$ CSNPs/rGO NCs (Fig. 1G), and the samples (Fig. 1B–E) are clearly identified using the standard patterns of cubic-structured Ni (JCPDS No. 70-0989) and Cu (JCPDS No. 89-2838). Peaks of impurities are not detected, which indicate the high purity of the samples. As shown in Fig. 1F and G, the proposed $Cu_{52}@Ni_{48}$ CSNPs and $Cu_{53}@Ni_{47}$ CSNPs/rGO NCs exhibit patterns corresponding to Ni (JCPDS No. 70-0989) and Cu (JCPDS No. 89-2838), which indicate that the Cu and Ni are separated phase in NPs. Graphite oxide is known to exhibit a sharp peak at $2\theta = 9.7°$, which corresponds to the (001) reflection of graphene oxide, and can be reduced to graphene during the *in situ* solvothermal process.[12a,b] Given that $Cu_{53}@Ni_{47}$ CSNPs are formed on graphene surface, the

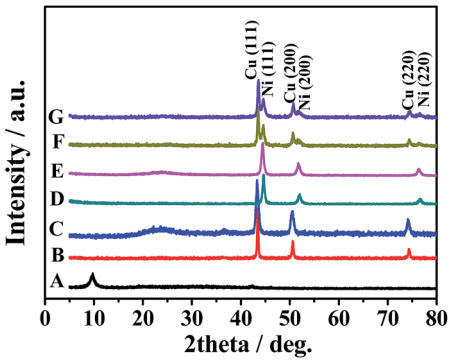

Fig. 1 XRD patterns of the obtained GO (A), Cu NPs (B), Cu/rGO NCs (C), Ni NPs (D), Ni/rGO NCs (E), $Cu_{52}@Ni_{48}$ CSNPs (F), and $Cu_{53}@Ni_{47}$ CSNPs/rGO NCs (G).

diffraction peaks from the stack rGO sheets almost disappear in the XRD pattern (Fig. 1G) of $Cu_{53}@Ni_{47}$ CSNPs/rGO hybrid NCs.

Raman spectroscope is a powerful technique for investigating the structural and electronic properties of carbon compounds. The significant structural changes occurring during the chemical processing from GO to rGO are also reflected in Raman spectra.[12] GO (Fig. S1, ESI†) displays two prominent peaks at 1347 and 1597 cm^{-1}, corresponding to the D and G bands, respectively. The G band is usually assigned to the plane bond stretching of the C–C sp^2 bond and D band is associated with structural defects and disorders.[12a] Here, the intensity ratio of D to G band (I_D/I_G) is used as a measure of structural defects and disorder in graphene structures,[12] and the I_D/I_G ratio varies from 1.12 for graphene oxide to 1.79 for the $Cu_{53}@Ni_{47}$ CSNPs/rGO NCs. The reason for increasing of I_D/I_G ratio is reasonable because after chemical reduction of GO. We can also observe that the G band of $Cu_{53}@Ni_{47}$ CSNPs/rGO NCs moves from 1597 to about 1578 cm^{-1}, close to the value of the pristine graphite.[12] Furthermore, we use XPS to characterize detailed information about the as-obtained $Cu_{53}@Ni_{47}$ CSNPs/rGO NCs. As shown in Fig. S2 (ESI†), the peaks locate at 853.2 and 870.9 eV are assigned to the metallic Ni, and the peak locate at 932.1 eV is assigned to the metallic Cu. Above results indicate that GO in $Cu_{53}@Ni_{47}$ CSNPs/rGO NCs has been well deoxygenated and reduced, and which support the results from XRD pattern (Fig. 1G).

Morphologies and sizes of the final products were observed *via* scanning electron microscopy (SEM). Fig. 2 shows the SEM images of Cu NPs (Fig. 2A), Cu/rGO (Fig. 2C), Ni NPs (Fig. 2B), Ni/rGO (Fig. 2D), $Cu_{52}@Ni_{48}$ CSNPs (Fig. 2E), and $Cu_{53}@Ni_{47}$ CSNPs/rGO NCs (Fig. 2F), and irregular particle morphologies are obtained for each sample. From the SEM images, we obtain the size distributions of Cu NPs, Cu/rGO, Ni NPs, Ni/rGO, $Cu_{52}@Ni_{48}$ CSNPs, and $Cu_{53}@Ni_{47}$ CSNPs/rGO were 120–250, 30–130, 20–120, 40–100, 50–110, and 35–110 nm, respectively. Transmission electron microscopy (TEM) was applied to characterize the $Cu_{53}@Ni_{47}$ CSNPs/rGO NCs. As shown in Fig. 3A, the rGO sheets are decorated with irregular NPs, which is consistent with SEM results (Fig. 2F). High resolution TEM (HRTEM, Fig. 3B) image indicate that the NPs with high crystallinity are

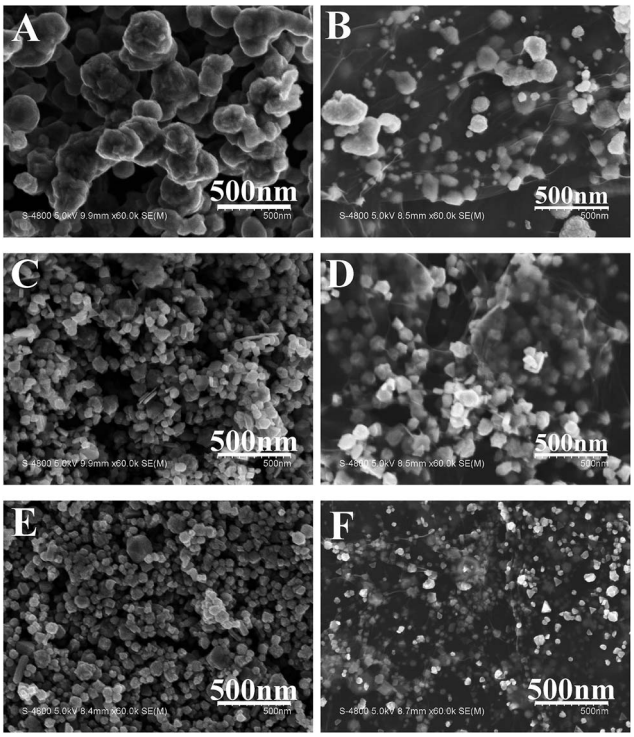

Fig. 2 Typical SEM images of (A) Cu NPs, (B) Cu/rGO NCs, (C) Ni NPs, (D) Ni/rGO NCs, (E) $Cu_{52}@Ni_{48}$ CSNPs, and (F) $Cu_{53}@Ni_{47}$ CSNPs/rGO NCs were obtained by solvothermal method.

observed. From the interior to exterior of the NPs, the two different fringe spacing are 0.21 nm (Fig. 3C) and 0.20 nm (Fig. 3D), and which correspond to the interplanar spacing of {111} planes for fcc Cu and fcc Ni, respectively. Thereby, energy-dispersive X-ray spectroscopy (EDS, which attached to JEOL JEM-2100F TEM) mapping was further used to reveal different elements distribution in the $Cu_{52}@Ni_{48}$ CSNPs/rGO NCs. Fig. 3E–H show dark-field TEM image together with the elemental maps of Cu and Ni in the NCs, and we clearly see that Cu is the core and Ni is the shell. Namely, the as-prepared Cu–Ni NPs in the NCs have a core–shell structure, and which is in accordance with the XRD (Fig. 1G) and HRTEM (Fig. 3B–D) results. By using the same element-mapping technique, the samples of $Cu_x@Ni_{100-x}$ CSNPs/rGO NCs with different Cu/Ni molar ratios and $Cu_{52}@Ni_{48}$ CSNPs without rGO sheets were also identified (Fig. S3, ESI†), and all results reveal that those samples with core–shell structures are obtained. Furthermore, the chemical compositions (atomic percent) of CSNPs and NCs were determined by inductively-coupled plasma-atomic emission spectroscopy (ICP-AES). Based on the ICP-AES results (Table S1, ESI†), Cu/Ni molar ratios on Cu@Ni CSNPs and Cu@Ni CSNPs/rGO NCs are 52 : 48 and 53 : 47, and which are close to the initial molar ratio of Cu^{2+} to Ni^{2+}. Meanwhile, the quality ratios of $m_{Cu/Ni}$ (wt%) to $m_{rGO\ sheets}$ (wt%) in all $Cu_x@Ni_{100-x}$ CSNPs/rGO NCs were also evaluated by ICP-AES analysis (Table S1, ESI†).

Generally, the Cu@Ni or Ni@Cu CS structures are prepared by electrodeposition process.[13] Here, a facile and one-pot solvothermal method is developed to prepare Cu@Ni NPs with CS

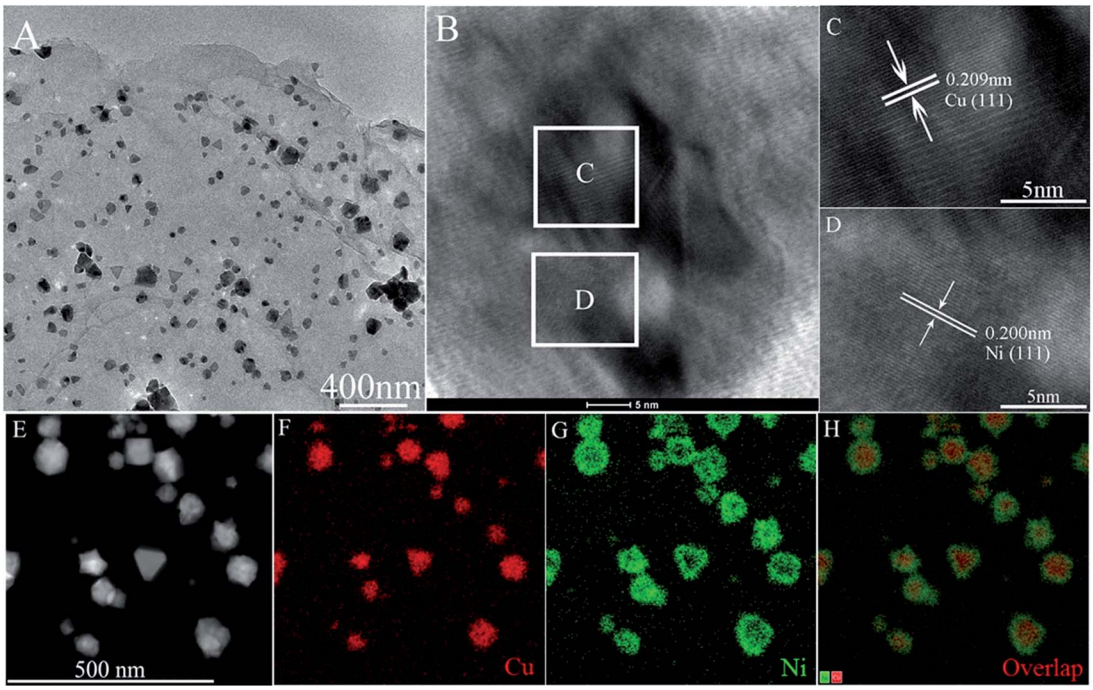

Fig. 3 TEM image (A), HRTEM images (B–D), HAADF-STEM image (E), STEM-EDX maps in Cu Kα1 signals (F) and Ni Kα1 signals (G), and overall map spectrum (H) of $Cu_{53}@Ni_{47}$ CSNPs/rGO NCs.

structure in this paper. Based on the above results, the possible growth process for the synthesis of $Cu_x@Ni_{100-x}$ CSNPs is discussed as follows. First, the GO sheets have big specific surface area and abundant functional groups,[9a,b,10] and the Cu^{2+} and Ni^{2+} can easy load on the surface of GO sheets by physical and chemical effects. And when the NaOH is added, Cu^{2+} and Ni^{2+} become the intermediate phase of $Cu(OH)_2$ and $Ni(OH)_2$, and then reduce to single metals by EG under alkaline condition. There are two key factors for controlling synthesis of Cu–Ni NPs with CS structures in this reaction system: enough potential difference in competitive redox reactions[13a,14] and moderate reductant (when the strong reductant of hydrazine hydrate is used, CuNi alloy is obtained).[12a] According to the redox potentials (−0.222 V for $Cu(OH)_2$/Cu and −0.72 V for $Ni(OH)_2$/Ni), the Cu^{2+} is reduced into Cu^0 at first,[13a,14] and next the Ni^{2+} is reduced into Ni^0 on the Cu surface. Therefore, Cu and Ni with CS structure NPs are formed. Simultaneously, the Cu–Ni NPs with CS structure (Fig. S3E_1–E_4, ESI†) are also obtained in the absence of GO sheets or other additives. This phenomenon reveals that Cu NPs not only act the load-island role, but also act interface catalyst for the next Ni nucleation on Cu NPs's surfaces. Thereby, the Cu–Ni NPs and Cu–Ni NPs in GO-based NCs with CS structures are successfully synthesized by this facile and one-pot solvothermal method.

Electrochemical behavior of $Cu_{53}@Ni_{47}$ CSNPs/rGO/Nafion/GCE

Normally, cyclic voltammetry is used to investigate electrochemical behavior of NCs. Here, the electrochemical properties of $Cu_{53}@Ni_{47}$ CSNPs/rGO NCs are also investigated by cyclic voltammetry in 0.1 M NaOH at different scan rates and the results are shown in Fig. 4A. When the scan rate is increased from 20 mV s^{-1} to 250 mV s^{-1} (Fig. 4B), both anodic and cathodic peak currents are found proportional to the scan rates with a linear equation of $i_{pa} = -3.487 - 0.016v$ ($R = 0.9996$, $n = 10$) and $i_{pc} = 2.418 + 0.009v$ ($R = 0.9986$, $n = 10$), respectively. These results indicate that the electrochemical kinetics of $Cu_{53}@Ni_{47}$ CSNPs/rGO/Nafion/GCE is surface controlled. The anodic peak potential shift more positively with increasing scan rates, whereas the cathodic potential shifted more negatively, which result in a larger peak-to-peak potential separation. These results are possibly due to NiO(OH) nucleation followed by increased active sites for both Ni^{3+} and Ni^{2+} species.[15]

Electrocatalytic oxidation of glucose on $Cu_{53}@Ni_{47}$ CSNPs/rGO/Nafion/GCE

A comparative study on the electrocatalytic performance toward glucose oxidation at different modified electrodes are carried out by cyclic voltammograms (CVs) in 0.1 M NaOH with and without 2 mM glucose at a scan rate of 50 mV s^{-1} (Fig. 5). As shown in Fig. 5A–F, the Cu/Nafion/GCE, Cu/rGO/Nafion/GCE, Ni/Nafion/GCE, Ni/rGO/Nafion/GCE, $Cu_{52}@Ni_{48}$ CSNPs/Nafion/GCE, and $Cu_{53}@Ni_{47}$ CSNPs/rGO/Nafion/GCE show an obvious oxidation peak toward glucose at +0.60 V, 0.55 V, +0.48 V, +0.47 V, +0.52 V, and +0.575 V, respectively. According to literatures,[1a,3a,16] the oxidation potentials of Cu- or Ni-based electrodes may be corresponded to a redox couple of Cu(II)/Cu(III) or Ni(II)/Ni(III). It is accepted that the oxidation of glucose to gluconolactone is catalyzed by Cu(II)/Cu(III) and Ni(II)/Ni(III) redox couples: CuO(OH) + glucose → $Cu(OH)_2$ + gluconolactone and NiO(OH) +

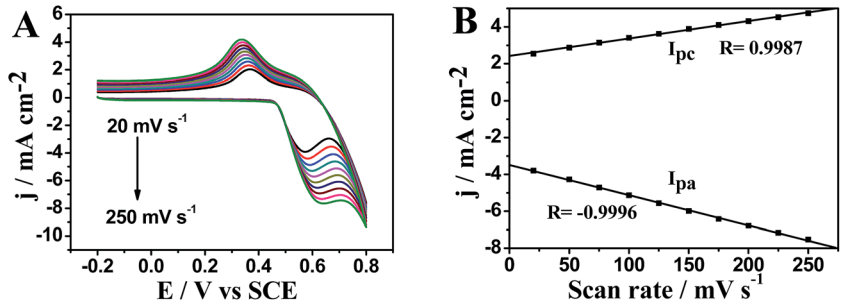

Fig. 4 (A) CVs of $Cu_{53}@Ni_{47}$ CSNPs/rGO/Nafion/GCE in 0.1 M NaOH at different scan rates: 20, 50, 75, 100, 125, 150, 175, 200, 225, and 250 mV s^{-1}. (B) Plot of peak current *versus* the potential scan rate.

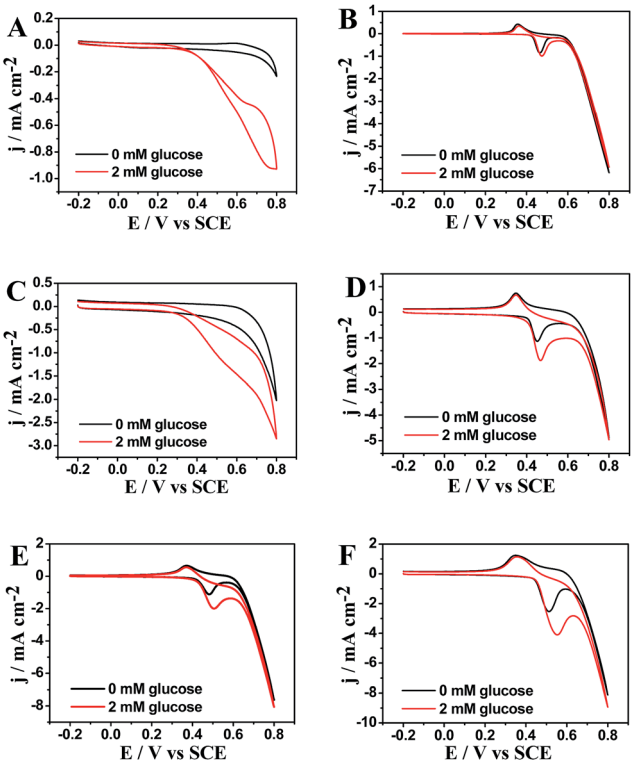

Fig. 5 CVs of (A) Cu/Nafion/GCE, (B) Ni/Nafion/GCE, (C) Cu/rGO/Nafion/GCE, (D) Ni/rGO/Nafion/GCE, (E) $Cu_{53}@Ni_{47}$ CSNPs/Nafion/GCE, and (F) $Cu_{53}@Ni_{47}$ CSNPs/rGO/Nafion/GCE examined in 0.1 M NaOH with absence/presence of 2 mM glucose at a scan rate of 50 mV s^{-1}.

glucose → $Ni(OH)_2$ + gluconolactone, respectively. This suggests that compositions of Cu and Ni play a major role in the oxidation of glucose. The $Cu_{53}@Ni_{47}$ CSNPs/rGO/Nafion/GCE also shows higher electrocatalytic oxidation to glucose than that of Cu/Nafion/GCE or Ni/Nafion/GCE. This is explained by the synergistic effect between $Cu_{53}@Ni_{47}$ CSNPs with rGO sheets on the oxidation of glucose. In absence of glucose, the background current of $Cu_{53}@Ni_{47}$ CSNPs/rGO/GCE (Fig. 5F) is higher than that of other modified electrodes (Fig. 5A–E), which indicate that $Cu_{53}@Ni_{47}$ CSNPs/rGO/GCE has the highest active surface area.

Up addition of glucose, Cu/rGO/Nafion/GCE, Ni/rGO/Nafion/GCE and $Cu_{53}@Ni_{47}$ CSNPs/rGO/Nafion/GCE exhibit enhanced glucose electrocatalytic oxidation with 2.7-, 1.4- and 2.9-fold higher electrochemical responses than that of Cu/Nafion/GCE, Ni/Nafion/GCE and $Cu_{52}@Ni_{48}$ CSNPs/Nafion/GCE respectively and display the substantially negative shift in peak potential. This result indicates that the higher current response is partially attributed to the high conductivity of the graphene sheets. The graphene-based modified electrode provide a more sterically hindered structure and a larger conducting surface area to support more active species.[9,17] In addition, the $Cu_{53}@Ni_{47}$ CSNPs/rGO/Nafion/GCE shows a uniquely high net current that is approximately 2.9 times greater than those in other modified electrodes. The much higher current response of the $Cu_{53}@Ni_{47}$ CSNPs/rGO/Nafion/GCE may be due to its uniform and compact structure. This rGO sheets provide a more conductive surface area to load $Cu_{53}@Ni_{47}$ CSNPs active species, resulting in a uniform, compact and active hybrid NCs. Thus, the NCs show specific activity toward glucose oxidation.

Bimetal molar ratio in NCs is a major parameter for active materials.[3e,6,11] Effects of Cu to Ni molar ratio on the catalytic performance of $Cu_x@Ni_{100-x}$ CSNPs/rGO/Nafion/GCE are also investigated. Table S2 (ESI†) shows the net current estimate on the electrocatalytic activity of the $Cu_x@Ni_{100-x}$ CSNPs/rGO/Nafion/GCE on glucose oxidation in the absence or presence of 0.5 mM glucose. The highest net current value is obtained from the 53 : 47 of Cu to Ni molar ratio, which suggests that the composite exhibits high activity toward glucose oxidation because of the synergistic effect of $Cu_{53}@Ni_{47}$ CS structure with rGO sheets. Moreover, this result also indicates that 53 : 47 is the optimum Cu to Ni molar ratio for the synthesis of active $Cu_{53}@Ni_{47}$ CSNPs/rGO NCs.

To improve the sensing performance of the electrode, the effect of applied potentials on sensor response is systematically investigated (Fig. S4, ESI†). Current–time curves are recorded at different applied potentials (+0.525 V to +0.625 V) with successive addition of 0.5 mM glucose to 0.1 M NaOH. The results illustrate that the maximum response is also observed at +0.575 V applied potential, and which is consistent with previous test (Fig. 5F). So, the +0.575 V is chosen as the optimal potential for amperometric glucose sensing due to this potential is strongly related to the oxidation peaks of Cu(II)/Cu(III) and Ni(II)/Ni(III).[6a–c,15,16]

Amperometric response of the $Cu_{53}@Ni_{47}$ CSNPs/rGO/Nafion/GCE towards glucose

The amperometric response of $Cu_{53}@Ni_{47}$ CSNPs/rGO/Nafion/GCE upon successive addition of different concentration of

glucose is further evaluated at the optimum experimental conditions. The modified electrode responds quickly to the change of glucose concentration and reaches about 95% of the steady-state current is no more than 3 s (inset in Fig. 6A) indicating an extraordinarily fast rapid and sensitive response to glucose. The calibration curve for the modified electrode is shown in Fig. 6B. The current response of the sensor exhibits a linear dependence on glucose concentration from 1 μM to 4.1 mM ($i = 0.08 + 0.78c$, $R = 0.9969$). The detection limit of glucose using a $Cu_{53}@Ni_{47}$ CSNPs/rGO/GCE is found to be 0.5 μM (S/N = 3) with the sensitivity of 780 μA mM^{-1} cm^{-2}. For comparison, the performances of other non-enzymatic glucose sensors based on reported in literatures have been listed in Table 1. It can be concluded that our sensor exhibits a very faster response, a lower detection limit and a wider linear range. These are attributed to the following reasons: (i) synergetic effect from bimetallic compositions.[6,11,19] Based on the above results, the electrocatalytic glucose oxidation ability decreased when the Cu/Ni molar ratio is too smaller or too higher, and the optimized Cu/Ni molar ratio resulting the high activity towards glucose oxidation. Thereby, the $Cu_{53}@Ni_{47}$ CSNPs/rGO/GCE exhibits high activity toward glucose oxidation. (ii) Synergetic effect from the specific CS structures.[14b,19] In the previous reports, the core–shell structure as a typical structure there are three major synergistic interactions (such as ligand effect, ensemble effects, and geometric effects) between the core and shell which resulting the enhanced electrocatalytic activity. Furthermore, the thickness of the Ni coating layer is importance to oxidation resistance. The molar ratio of Cu to Ni is 53 : 47 reveals a highest electrocatalytic activity for $Cu_{53}@Ni_{47}$ CSNPs/rGO NCs. (iii) Synergetic effect between the NPs and support materials.[6,11,17,19] Cu@Ni CSNPs decorating the reduced graphene oxide sheets on the electrode surface, which significantly increases the number of electrocatalytic active areas and promotes electron transfer in the oxidation of glucose.

Table 1 Comparison of the performances of our Cu@Ni CSNPs/rGO sensor with other published non-enzymatic glucose sensors

Electrode material	Linear range (mM)	Detection limit (μM)	Reference
$Cu_{53}@Ni_{47}$ CSNPs/rGO NCs	0.001–4.1	0.5	This work
PdCu/GE	1–18	20	6a
ITO/Ni/Cu	0.001–2	0.23	6b
Ni–Cu/TiO_2NTs	0.01–3.2	5	6c
Pt/Ni NWAs	0–2	1.5	6f
Ni–Co NSs/rGO	0.01–2.65	3.79	11a
Cu–Co NSs/rGO–CHIT	0.015–6.95	10	11b
Ni NPs/SMWNTs	0.001–1	0.5	16
rGO–Ni NPs	0.002–2.1	0.1	18a
BDD/Ni	0.005–10	2.7	18b
Ni–CNF	1–10	—	18c
Cu NPs–GR	0.01–1.2	3.4	18d
Cu/PMo12-GR	0.0001–1.0	0.03	18e

Reproducibility, stability and anti-interference property of the $Cu_{53}@Ni_{47}$ CSNPs/rGO/Nafion/GCE

The reproducibility of $Cu_{53}@Ni_{47}$ CSNPs/rGO/Nafion/GCE is examined by measuring its amperometric response to 0.5 mM glucose. A 3.4% relative standard deviation is obtained from 10 successive amperometric determinations, which indicates a relatively good reproducibility. The stability of the modified electrode is evaluated by storing it for 72 h at 4 °C. The response current is maintained at 93.0% of its initial response, which demonstrates a good stability, whereas $Cu_{53}@Ni_{47}$ CSNPs/rGO/Nafion/GCE retains 89% of its initial current value, which clearly confirms the importance of the graphene scaffold in enhancing the stability of $Cu_{53}@Ni_{47}$ CSNPs.

The anti-interference property and stability of $Cu_{53}@Ni_{47}$ CSNPs/rGO/Nafion/GCE are crucial in developing nonenzymatic electrochemical biosensors. Given that chemical species such as uric acid (UA), dopamine (DA), ascorbic acid (AA), and NaCl that easily oxidize are always present with glucose in human blood, their electrochemical response are also examined using $Cu_{53}@Ni_{47}$ CSNPs/rGO/Nafion/GCE. The normal physiological glucose level is considered to be considerably higher than the above analytes.[20] In the present study, the interference experiment is conducted by adding 0.1 mM interfering species into 0.5 mM glucose in 0.1 M NaOH. As shown in Fig. S5 (ESI†), there is no obvious current response observed with the addition of 0.1 mM DA, 0.1 mM UA and 0.1 mM AA. Moreover, the addition of NaCl does not show any effect on the current of glucose oxidation, suggesting high chloride tolerance of $Cu_{53}@Ni_{47}$ CSNPs/rGO/Nafion/GCE. Furthermore, the response of other

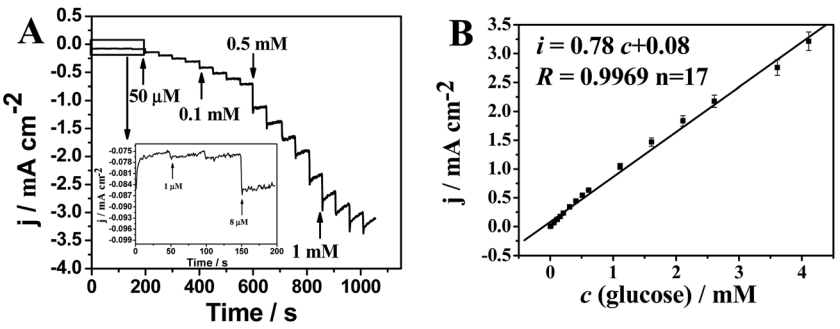

Fig. 6 (A) Current–time responses at +0.575 V with an increasing glucose concentration per 50 s for the $Cu_{53}@Ni_{47}$ CSNPs/rGO/Nafion/GCE. (B) The linear relationship between the catalytic current and glucose concentration.

Table 2 Determination of glucose concentration in the simulative sample ($n = 3$)

Sample	Add (mM)	Found (mM)	Recovery (%)	R.S.D. (%, $n = 3$)
1	0.5	0.476	95.2	4.12
2	0.6	0.627	104.3	4.69

sugars, such as 0.5 mM glucose, 0.1 mM sucrose, 0.1 mM maltose, 0.1 mM fructose, 0.1 mM D-galactose, 0.5 mM glucose compares to that of glucose, is also evaluated as shown in Fig. S6 (ESI†). Current responses of the corresponding interfering species are also very weak, and demonstrate that the low level of saccharides will not affect the detection of glucose by this excellent sensor. Overall, it can be concluded that the small amounts of interfering species have a weakly influence on the glucose response. In other words, the $Cu_{53}@Ni_{47}$ CSNPs/rGO/Nafion/GCE shows high selectivity for glucose detection.

Simulative sample analysis

However, despite the complexity of the serum components, only glucose, AA, and UA are electrochemically active. Therefore, a simulative serum sample containing 1 mM glucose, 0.08 mM AA, and 0.04 mM UA is prepared according to the approximate concentrations of the three components in an actual 20% serum sample.[21] Glucose is evaluated in the simulated serum by using $Cu_{53}@Ni_{47}$ CSNPs/rGO/Nafion/GCE; the results are listed in Table 2. The results show that other electroactive components in serum do not significantly interfere with the glucose determination. Hence, the $Cu_{53}@Ni_{47}$ CSNPs/rGO/Nafion/GCE can be potentially used for routine blood glucose testing.

4 Conclusions

In summary, the $Cu_x@Ni_{100-x}$ (x = 70, 63, 53, 38, and 20) CSNPs/rGO NCs are synthesized by a facile and one-pot solvothermal method. We demonstrate that $Cu_{53}@Ni_{47}$ CSNPs/rGO/GCE shows the highest electrochemical response towards glucose oxidation due to the three-in-one synergistic effects from Cu/Ni bimetallic system, Cu@Ni core–shell structure, and interactions from the bimetallic CSNPs and reduced graphene oxide sheets. $Cu_{53}@Ni_{47}$ CSNPs/rGO/GCE reveals a low cost, high sensitivity, and good reproducibility in glucose determination. A wide linear range of 0.001 to 4.1 mM, a low detection limit of 0.5 μM (S/N = 3), a high sensitivity of 780 μA mM^{-1} cm^{-2}, and a fast response time (3 s) are obtained. Furthermore, the oxidable species shows insignificant interference in determination of glucose, and which indicates that $Cu_{53}@Ni_{47}$ CSNPs/rGO NCs-based sensor has potential applications for the determination of glucose in biological fluids.

Acknowledgements

This work is financially supported by the National Natural Science Foundation of China (Nos 21501004, 21071005, 21271006, 21201008), and the Research Culture Funds of Anhui Normal University (No. 2014xmpy13), and the Innovation Funds of Anhui Normal University (No. 2014cxjj13).

References

1 (*a*) G. F. Wang, X. P. He, L. L. Wang, A. X. Gu, Y. Huang, B. Fang, B. Y. Geng and X. J. Zhang, *Microchim. Acta*, 2013, **180**, 161; (*b*) A. Heller and B. Feldman, *Chem. Rev.*, 2008, **108**, 2482; (*c*) J. Wang, *Chem. Rev.*, 2008, **108**, 814; (*d*) C. Chen, Q. J. Xie, D. W. Yang, H. L. Xiao, Y. C. Fu, Y. M. Tan and S. Z. Yao, *RSC Adv.*, 2013, **3**, 4473; (*e*) X. Niu, X. Li, J. Pan, Y. He, F. Qiu and Y. Yan, *RSC Adv.*, 2016, **6**, 84893.

2 (*a*) L. Su, X. Yu, W. Qin, W. Dong, C. Wu, Y. Zhang, G. Mao and S. Feng, *J. Mater. Chem. B*, 2017, **5**, 116; (*b*) P. Si, Y. J. Huang, T. H. Wang and J. M. Ma, *RSC Adv.*, 2013, **3**, 3487; (*c*) L. Pu, M. Baig and V. Maheshwari, *Anal. Bioanal. Chem.*, 2016, **408**, 2697.

3 (*a*) Y. Yang, Y. Wang, X. Bao and H. Li, *J. Electroanal. Chem.*, 2016, **775**, 163; (*b*) L. Wang, X. Lu, C. Wen, Y. Xie, L. Miao, S. Chen, H. Li, P. Li and Y. Song, *J. Mater. Chem. A*, 2015, **3**, 608; (*c*) S.-J. Li, N. Xia, X.-L. Lv, M.-M. Zhao, B.-Q. Yuan and H. Pang, *Sens. Actuators, B*, 2014, **190**, 809; (*d*) A. Rengaraj, Y. Haldorai, C. H. Kwak, S. Ahn, K.-J. Jeon, S. H. Park, Y.-K. Han and Y. S. Huh, *J. Mater. Chem. B*, 2015, **3**, 6301; (*e*) W. Yan, D. Wang and G. G. Botte, *Electrochim. Acta*, 2012, **61**, 25; (*f*) B. Yuan, C. Xu, D. Deng, Y. Xing, L. Liu, H. Pang and D. Zhang, *Electrochim. Acta*, 2013, **88**, 708; (*g*) Z. Liu, Y. Guo and C. Dong, *Talanta*, 2015, **137**, 87.

4 (*a*) Y. Li, J. J. Fu, R. S. Chen, M. Huang, B. Gao, K. F. Huo, L. Wang and P. K. Chu, *Sens. Actuators, B*, 2014, **192**, 474; (*b*) J. Zhao, L. Wei, C. Peng, Y. Su, Z. Yang, L. Zhang, H. Wei and Y. Zhang, *Biosens. Bioelectron.*, 2013, **47**, 86; (*c*) A. A. Ensafi, M. Jafari-Asl, N. Dorostkar, M. Ghiaci, M. V. Martínez-Huert and J. L. G. Fierro, *J. Mater. Chem. B*, 2014, **2**, 706; (*d*) X. Lu, Y. Ye, Y. Xie, Y. Song, S. Chen, P. Li, L. Chen and L. Wang, *Anal. Methods*, 2014, **6**, 4643; (*e*) L. Liu, Y. Chen, H. Lv, G. Wang, X. Hu and C. Wang, *J. Solid State Electrochem.*, 2015, **19**, 731; (*f*) Q. Wang, Q. Wang, M. Li, S. Szunerits and R. Boukherroub, *RSC Adv.*, 2015, **5**, 15861; (*g*) J. Zheng, W. Zhang, Z. Lin, C. Wei, W. Yang, P. Dong, Y. Yan and S. Hu, *J. Mater. Chem. B*, 2016, **4**, 1247.

5 C. M. Welch and R. G. Compton, *Anal. Bioanal. Chem.*, 2006, **384**, 601.

6 (*a*) M. Yuan, A. P. Liu, M. Zhao, W. J. Dong, T. Y. Zhao, J. J. Wang and W. H. Tang, *Sens. Actuators, B*, 2014, **190**, 707; (*b*) P. Salazar, V. Rico and A. R. González-Elipe, *Sens. Actuators, B*, 2016, **226**, 436; (*c*) X. L. Li, J. Y. Yao, F. L. Liu, H. C. He, M. Zhou, N. Mao, P. Xiao and Y. H. Zhang, *Sens. Actuators, B*, 2013, **181**, 501; (*d*) K. C. Lin, Y. C. Lin and S. M. Chen, *Electrochim. Acta*, 2013, **96**, 164; (*e*) H.-B. Noh, K.-S. Lee, P. Chandra, M.-S. Won and Y.-B. Shim, *Electrochim. Acta*, 2012, **61**, 36; (*f*) S. S. Mahshid, S. Mahshid, A. Dolati, M. Ghorbani, L. Yang, S. Luo and Q. Cai, *Electrochim. Acta*, 2011, **58**, 551.

7 (*a*) M. B. Gawande, A. Goswami, T. Asefa, H. Guo, A. V. Biradar, D.-L. Peng, R. Zboril and R. S. Varma, *Chem. Soc. Rev.*, 2015, **44**, 7540; (*b*) Y. Holade, A. Lehoux, H. Remita, K. B. Kokoh and T. W. Napporn, *J. Phys. Chem. C*, 2015, **119**, 27529; (*c*) J. Wang, L. Xu, Y. Lu, K. Sheng, W. Liu, C. Chen, Y. Li, B. Dong and H. Song, *Anal. Chem.*, 2016, **88**, 12346.

8 (*a*) C. Zhao, P. Gai, R. Song, J. Zhang and J.-J. Zhu, *Anal. Methods*, 2015, **7**, 4640; (*b*) G.-H. Yang, Y.-H. Zhou, J.-J. Wu, J.-T. Cao, L.-L. Li, H.-Y. Liu and J.-J. Zhu, *RSC Adv.*, 2013, **3**, 22597; (*c*) G. Yang, Y. Li, R. K. Rana and J.-J. Zhu, *J. Mater. Chem. A*, 2013, **1**, 1754; (*d*) Y. Chen, Y. Li, D. Sun, D. Tian, J. Zhang and J.-J. Zhu, *J. Mater. Chem.*, 2011, **21**, 7604; (*e*) J. J. Gooding, *Electrochim. Acta*, 2005, **50**, 3049; (*f*) H. Sun, J. Ren and X. Qu, *Acc. Chem. Res.*, 2016, **49**, 461; (*g*) K. Qu, L. Wu, J. Ren and X. Qu, *ACS Appl. Mater. Interfaces*, 2012, **4**, 5001; (*h*) M. Li, Y. Guan, C. Ding, Z. Chen, J. Ren and X. Qu, *J. Mater. Chem. B*, 2016, **4**, 4072; (*i*) L. Wu, L. Feng, J. Ren and X. Qu, *Biosens. Bioelectron.*, 2012, **34**, 57.

9 (*a*) D. Chen, L. Tang and J. Li, *Chem. Soc. Rev.*, 2010, **39**, 3157; (*b*) D. Chen, H. Feng and J. Li, *Chem. Rev.*, 2012, **112**, 6027; (*c*) R. Que, Q. Shao, Q. Li, M. Shao, S. Cai, S. Wang and S. T. Lee, *Angew. Chem., Int. Ed.*, 2012, **51**, 5418; (*d*) A. Rengaraj, Y. Haldorai, C. H. Kwak, S. Ahn, K.-J. Jeon, S. H. Park, Y.-K. Han and Y. S. Huh, *J. Mater. Chem. B*, 2015, **3**, 6301; (*e*) S. Pattnaik, K. Swain and Z. Lin, *J. Mater. Chem. B*, 2016, **4**, 7813; (*f*) B. Thirumalraj, C. Rajkumar, S.-M. Chen and P. Barathi, *J. Mater. Chem. B*, 2016, **4**, 6335; (*g*) S.-J. Li, Y.-F. Shi, L. Liu, L.-X. Song, H. Pang and J.-M. Du, *Electrochim. Acta*, 2012, **85**, 628; (*h*) S. Zhuo, M. Shao and S.-T. Lee, *ACS Nano*, 2012, **6**, 1059.

10 (*a*) S. Bong, Y. R. Kim, I. Kim, S. Woo, S. Uhm, J. Lee and H. Kim, *Electrochem. Commun.*, 2010, **12**, 129; (*b*) X. W. Liu, J. J. Mao, P. D. Liu and X. W. Wei, *Carbon*, 2011, **49**, 477; (*c*) X.-W. Liu, Z.-J. Yao, Y.-F. Wang and X.-W. Wei, *Colloids Surf., B*, 2010, **81**, 508.

11 (*a*) L. Wang, X. P. Lu, Y. J. Ye, L. L. Sun and Y. H. Song, *Electrochim. Acta*, 2013, **114**, 484; (*b*) L. Wang, Y. L. Zheng, X. P. Lu, Z. Li, L. L. Sun and Y. H. Song, *Sens. Actuators, B*, 2014, **195**, 1.

12 (*a*) J. Yang, X. Shen, Z. Ji, H. Zhou, G. Zhu and K. Chen, *Appl. Surf. Sci.*, 2014, **316**, 575; (*b*) J. Yang, X. Shen, Z. Ji, H. Zhou, G. Zhu and K. Chen, *Ceram. Int.*, 2015, **41**, 4056; (*c*) Z. Zafar, Z. H. Ni, X. Wu, Z. X. Shi, H. Y. Nan, J. Bai and L. T. Sun, *Carbon*, 2013, **61**, 57; (*d*) S. Stankovich, D. A. Dikin, R. D. Piner, K. A. Kohlhaas, A. Kleinhammes, Y. Jia, Y. Wu, S. T. Nguyen and R. S. Ruoff, *Carbon*, 2007, **45**, 1558; (*e*) B. Li, H. Cao, J. Yin, Y. A. Wu and J. H. Warner, *J. Mater. Chem.*, 2012, **22**, 1876.

13 (*a*) Z. Liu, L. Guo, C.-L. Chien and P. C. Searson, *J. Electrochem. Soc.*, 2008, **155**, D569; (*b*) Z. Liu, G. Xia, F. Zhu, S. Kim, N. Markovic, C.-L. Chien and P. C. Searson, *J. Appl. Phys.*, 2008, **103**, 064313; (*c*) Z. Liu, D. Elbert, C.-L. Chien and P. C. Searson, *Nano Lett.*, 2008, **8**, 2166; (*d*) M. Hennes, J. Buchwald and S. G. Mayr, *CrystEngComm*, 2012, **14**, 7633; (*e*) M. Hennes, J. Buchwald, U. Ross, A. Lotnyk and S. G. Mayr, *Phys. Rev. B: Condens. Matter Mater. Phys.*, 2015, **91**, 245401.

14 (*a*) T. Yamauchi, Y. Tsukahara, T. Sakata, H. Mori, T. Yanagida, T. Kawai and Y. Wada, *Nanoscale*, 2010, **2**, 515; (*b*) J. Chen, J. Chen, Y. Li, W. Zhou, X. Feng, Q. Huang, J.-G. Zheng, R. Liu, Y. Ma and W. Huang, *Nanoscale*, 2015, **7**, 16874; (*c*) J. Feng and C. P. Zhang, *J. Colloid Interface Sci.*, 2006, **293**, 414; (*d*) S. Zhang and H. C. Zeng, *Chem. Mater.*, 2009, **21**, 871.

15 (*a*) M. Jafarian, M. G. Mahjani, H. Heli, F. Gobal and M. Heydarpoor, *Electrochem. Commun.*, 2003, **5**, 184; (*b*) B. Ballarin, R. Seeber, D. Tonelli and A. Vaccari, *J. Electroanal. Chem.*, 1999, **463**, 123.

16 H. G. Nie, Z. Yao, X. M. Zhou, Z. Yang and S. M. Huang, *Biosens. Bioelectron.*, 2011, **30**, 28.

17 (*a*) V. Georgakilas, M. Otyepka, A. B. Bourlinos, V. Chandra, N. Kim, K. C. Kemp, P. Hobza, R. Zboril and K. S. Kim, *Chem. Rev.*, 2012, **112**, 6156; (*b*) F. Xiao, J. Song, H. Gao, X. Zan, R. Xu and H. Duan, *ACS Nano*, 2012, **6**, 100.

18 (*a*) Y. Zhang, X. Xiao, Y. Sun, Y. Shi, H. Dai, P. Ni, J. Hu, Z. Li, Y. Song and L. Wang, *Electroanalysis*, 2013, **25**, 959; (*b*) Y. Liu, H. Teng, H. Hou and T. You, *Biosens. Bioelectron.*, 2009, **24**, 3329; (*c*) K. E. Toghill, L. Xiao, M. A. Phillips and R. G. Compton, *Sens. Actuators, B*, 2010, **147**, 642; (*d*) P. Salazar, V. Rico, R. Rodríguez-Amaro, J. P. Espinós and A. R. González-Elipe, *Electrochim. Acta*, 2015, **169**, 195; (*e*) W.-Y. Jeon, Y.-B. Choi and H.-H. Kim, *Sensors*, 2015, **15**, 31083.

19 K. D. Gilroy, A. Ruditskiy, H.-C. Peng, D. Qin and Y. Xia, *Chem. Rev.*, 2016, **116**, 10414.

20 J. P. Wang, D. F. Thomas and A. C. Chen, *Anal. Chem.*, 2008, **80**, 997.

21 Y. Q. Yang, C. L. Yi, J. Luo, R. Liu, J. K. Liu, J. Q. Jiang and X. Y. Liu, *Biosens. Bioelectron.*, 2011, **26**, 2607.